ular-electronics components based on metallic tubes are preferred. The present work shows that short, metallic nanotubes can be applied as RTSETs. It also serves to illustrate that the search for functional molecular devices often yields interesting fundamental science.

References and Notes

1. H. Grabert, M. Devoret, Eds., in *Single Charge Tunneling* (Plenum, New York, 1992).
2. Y. Takahashi *et al.*, *Electron. Lett.* **31**, 136 (1995).
3. K. Matsumoto *et al.*, *Appl. Phys. Lett.* **68**, 34 (1996).
4. L. Zhuang, L. Guo, S. Y. Chou, *Appl. Phys. Lett* **72**, 1205 (1998).
5. C. Dekker, *Phys. Today* **52** (5), 22 (1999).
6. H. W. Ch. Postma, M. de Jonge, Z. Yao, C. Dekker, *Phys. Rev. B* **62**, R10653 (2000).
7. H. W. Ch. Postma, A. Sellmeijer, C. Dekker, *Adv. Mater.* **17**, 1299 (2000).
8. C. W. J. Beenakker, *Phys. Rev. B* **44**, 1646 (1991).
9. S. J. Tans *et al.*, *Nature* **386**, 474 (1997).
10. M. Bockrath *et al.*, *Science* **275**, 1922 (1997).
11. D. H. Cobden, M. Bockrath, P. L. McEuen, A. G. Rinzler, R. E. Smalley, *Phys. Rev. Lett.* **81**, 681 (1998).
12. H. W. Ch. Postma, Z. Yao, C. Dekker, *J. Low Temp. Phys.* **118**, 495 (2000).
13. M. Bockrath *et al.*, *Science* **291**, 283 (2001).
14. M. Bockrath *et al.*, *Nature* **397**, 598 (1999).
15. Z. Yao, H. W. Ch. Postma, L. Balents, C. Dekker, *Nature* **402**, 273 (1999).
16. J. Nygard, D. H. Cobden, M. Bockrath, P. L. McEuen, P. E. Lindelof, *Appl. Phys. A* **69**, 297 (1999).
17. C. L. Kane, L. Balents, M. P. A. Fisher, *Phys. Rev. Lett.* **79**, 5086 (1997).
18. R. Egger, A. O. Gogolin, *Phys. Rev. Lett.* **79**, 5082 (1997).
19. C. L. Kane, M. P. A. Fisher, *Phys. Rev. Lett.* **68**, 1220 (1992).
20. A. Furusaki, *Phys. Rev. B.* **57**, 7141 (1998).
21. A. Braggio, M. Grifoni, M. Sassetti, F. Napoli, *Europhys. Lett.* **50**, 236 (2000).
22. Although the first theoretical predictions for Luttinger liquid behavior considered double-barrier devices, experimental evidence so far is scarce [see (*30*)].
23. M. P. A. Fisher, L. Balents, personal communication.
24. M. Grifoni *et al.*, unpublished data.
25. H. W. Ch. Postma, data not shown.
26. A. B. Zorin *et al.*, *Phys. Rev. B* **53**, 13682 (1996).
27. S. J. Tans, A. R. M. Verschueren, C. Dekker, *Nature* **393**, 49 (1998).
28. S. J. Tans, C. Dekker, *Nature* **404**, 834 (2000).
29. A. Bachtold *et al.*, *Phys. Rev. Lett.* **84**, 6082 (2000).
30. O. Auslaender *et al.*, *Phys. Rev. Lett.* **84**, 1764 (2000).
31. S. Iijima, C. Brabec, A. Maiti, J. Bernholc, *J. Chem. Phys.* **104**, 2089 (1996).
32. We thank R. E. Smalley and co-workers for providing the carbon nanotube material; A. Bachtold, M. P. A. Fisher, L. Balents, P. Hadley, M. Thorwart, A. Braggio, and Yu. V. Nazarov for discussions; and B. van den Enden for technical assistance. Supported by the Dutch Foundation for Fundamental Research on Matter (FOM) and the European Community SATURN project.

20 April 2001; accepted 23 May 2001

Fully Conjugated Porphyrin Tapes with Electronic Absorption Bands That Reach into Infrared

Akihiko Tsuda and Atsuhiro Osuka*

Scandium(III)-catalyzed oxidation of *meso-meso*–linked zinc(II)-porphyrin arrays (up to dodecamers) with 2,3-dichloro-5,6-dicyano-1,4-benzoquinone (DDQ) led to efficient formation of triply *meso-meso*–, β-β–, and β-β–linked zinc(II)-oligoporphyrins with 62 to 91% yields. These fused tape-shaped porphyrin arrays display extremely red-shifted absorption bands that reflect extensively π-conjugated electronic systems and a low excitation gap. The lowest electronic absorption bands become increasingly intensified and red-shifted upon the increase in the number of porphyrins and eventually reach a peak electronic excitation for the dodecamer at ~3500 wavenumber. The one-electron oxidation potentials also decreased progressively upon the increase in the number of porphyrins. These properties in long and rigid molecular shapes suggest their potential use as molecular wires.

Discrete molecules with a very long π-system are of interest as organic conducting materials, near-infrared (near-IR) dyes, nonlinear optical materials, and molecular wires (*1–3*). Numerous attempts that have been made to extend the π-electronic systems have, however, encountered serious problems, such as synthetic inaccessibility, chemical instability, poor solubility, and conjugation saturation behavior that arises through the effective conjugated length (ECL) effect. The ECL defines the extent of π-conjugated systems in which the electronic delocalization is limited and at which point the optical, electrochemical, and other physical properties reach a saturation level that is common with the analogous polymer (*1*). A straightforward strategy for maximizing π-overlap may be to hold the π-systems coplanar within a tapelike framework by fusing the units edge-to-edge, to make a covalently linked long, flat array, but this goal is synthetically quite demanding. Fused π-conjugated systems are promising also in circumventing the above ECL limit, as seen for the [*n*]acene series ($n = 1$ to 7) (*1*, *4*), but extension to the higher conjugated systems suffers from problems of poor solubility caused by the resulting planar structures. Within a confined pigment number, charged dyes such as oxonols and cyanines can escape the ECL effect because of the absence of the bond alternation arising from effective resonance (*5*). Again, extension to the higher homologs is difficult to achieve and reveals the ECL effect (*6*).

Porphyrins are intriguing building units from which to construct large π-conjugated molecules. Two types of conjugated porphyrins have been developed, *meso*-ethyne–bridged and *meso*-butadiyne–bridged porphyrin arrays (*7–9*) and fused porphyrin arrays (*10–13*), both of which show unusual properties that result from strong π-conjugation. Here we report the synthesis of highly conjugated porphyrin arrays, in which the electronic π-conjugation over the arrays is far stronger than the π-conjugation of these precedents, as seen from extremely low-energy IR electronic excitations.

Recently, we reported the synthesis of *meso-meso*–linked porphyrin arrays of up to 128-oligomers by Ag^I salt–promoted coupling reaction (*14*). This extremely long, discrete, rodlike organic molecule has a molecular length of about 108 nm. These arrays adopt a nearly orthogonal conformation that tends to minimize the electronic interaction between the neighboring porphyrins (*14*, *15*). The aryl-end–capped *meso-meso*–linked Cu^{II}-diporphyrin **1** can be converted to triply linked fused diporphyrin **2** by the oxidative double-ring closure (ODRC) reaction upon treatment with (p-$BrC_6H_4)_3NSbCl_6$ in C_6F_6 (Scheme 1) (*13*). The planar structure of **2** has been revealed by x-ray analysis, and full conjugation over the two porphyrins has been demonstrated by its substantially broadened and red-shifted absorption spectrum.

We now describe a highly efficient synthetic method that allows the ODRC reaction of higher *meso-meso*–linked Zn(II)-porphyrins in good yields. The ODRC reaction was conducted simply by refluxing a toluene solution of *meso-meso*–linked Zn(II)-diporphyrin **3** in the presence of five equivalents of 2,3-dichloro-5,6-dicyano-1,4-benzoquinone (DDQ) and scandium trifluoromethanesulfonate [$Sc(OTf)_3$] for 0.5 hour, which afforded the triply linked fused diporphyrin **4** in 86% yield as a sole product. DDQ or $Sc(OTf)_3$ alone did not effect any change of **3**. Under similar conditions, the Zn(II)-porphyrin monomer **5** was also effectively coupled to give triply linked diporphyrin **4** in

---

Department of Chemistry, Graduate School of Science, Kyoto University, Sakyo-ku, Kyoto 606-8502, Japan.

*To whom correspondence should be addressed.

an almost quantitative yield. The undesirable chlorination at the peripheral β positions, a serious problem in the ODRC reaction with (p-$BrC_6H_4)_3NSbCl_6$ (*13*), was completely suppressed. More important, the ODRC reaction was successfully applied to the synthesis of higher fused porphyrin arrays as follows: **13** (dimer, 75%) from **6**; **14** (trimer, 91%) from **7**; **15** (tetramer, 78%) from **8**; **16** (pentamer, 77%) from **9**; **17** (hexamer, 85%) from **10**; **18** (octamer, 60%) from **11**; and **19**

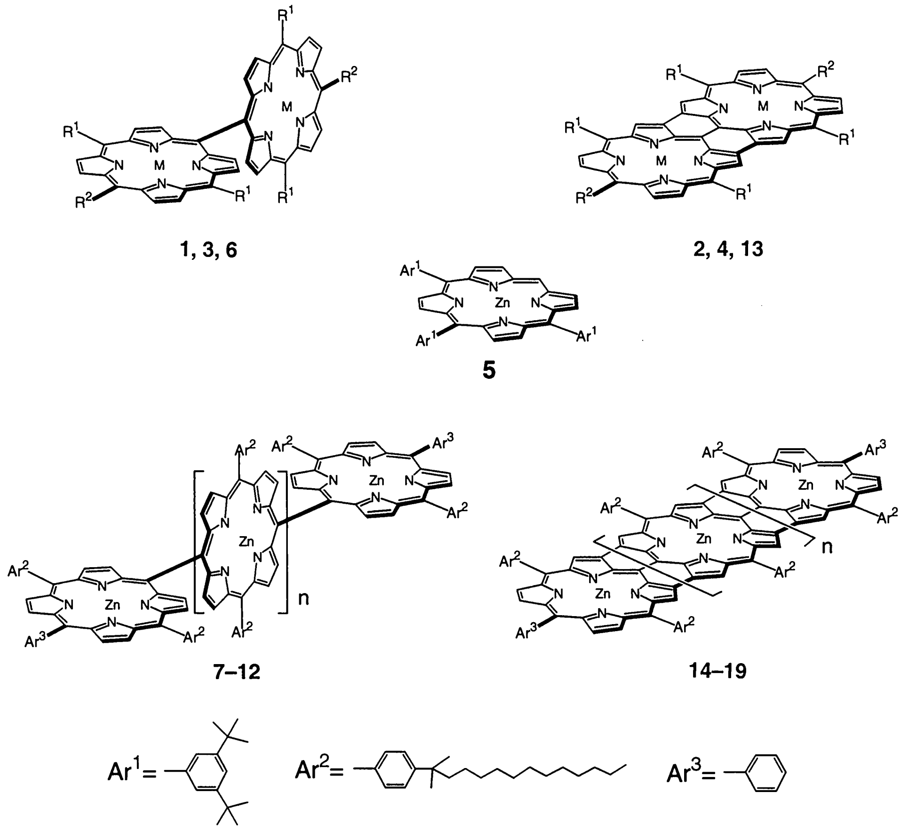

Scheme 1. **1**, M = Cu, R^1 = R^2 = Ar^1; **3**, M = Zn, R^1 = R^2 = Ar^1; **6**, M = Zn, R^1 = Ar^2, R^2 = Ar^3; **2**, M = Cu, R^1 = R^2 = Ar^1; **4**, M = Zn, R^1 = R^2 = Ar^1; **13**, M = Zn, R^1 = Ar^2, R^2 = Ar^3. Number of porphyrins (N): **7** (1), **8** (2), **9** (3), **10** (4), **11** (6), **12** (10); **14** (1), **15** (2), **16** (3), **17** (4), **18** (6), and **19** (10).

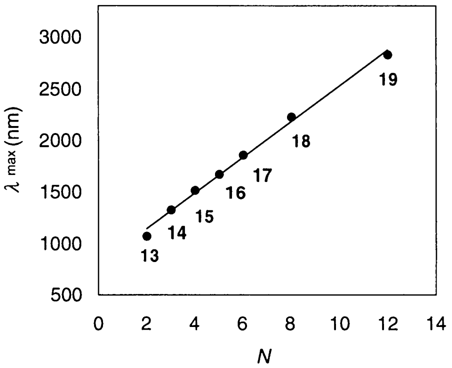

Fig. 2. Plot of absorption peak of bands III versus the numbers of porphyrins in the triply linked fused arrays (N). The line shown is represented by the equation λ_{max} = 174.5N + 793 (nm) with coefficient of variation r^2 = 0.995.

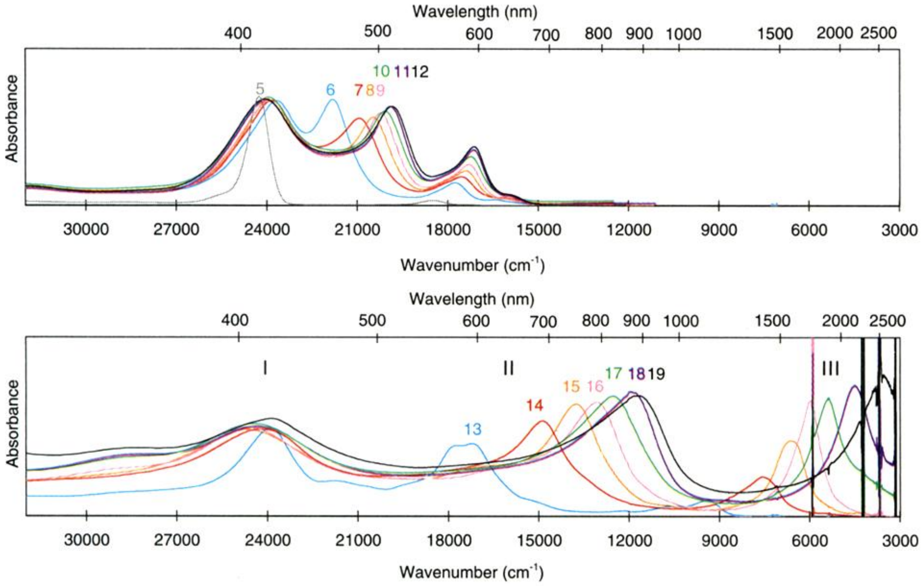

Fig. 1. Ultraviolet-visible-infrared absorption spectra of porphyrin **5** and *meso-meso*–linked porphyrin arrays **6** to **12** (top) and triply linked fused porphyrin arrays **13** to **19** (bottom) taken in $CHCl_3$ at room temperature. The absorption spectra of **5** to **12** and **13** to **19** were normalized at 23,700 to 24,000 cm^{-1} and 23,800 to 24,600 cm^{-1}, respectively. The background absorbance at ~6000, ~4000, and ~3500 cm^{-1} may arise from the overtones of C-H vibration of the solvent.

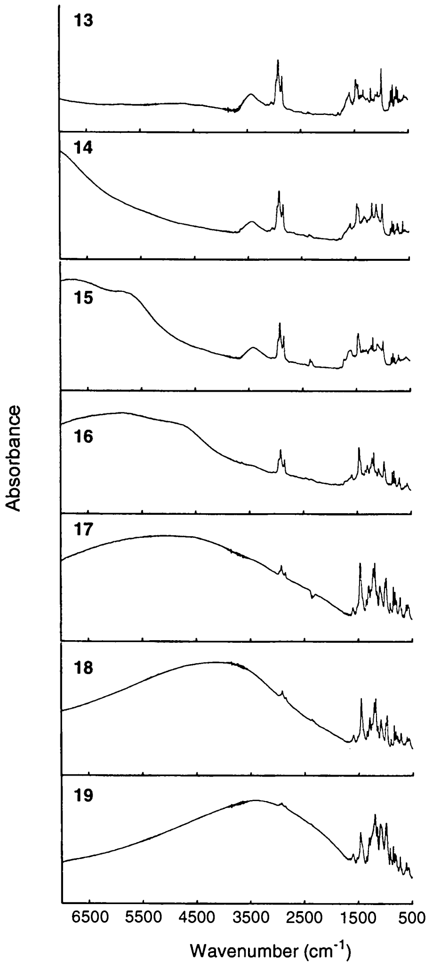

Fig. 3. IR spectra of molecules **13** to **19** taken in a KBr pellet at room temperature with a JASCO-FT-IR 420 spectrometer at room temperature.

(dodecamer, 73%) from **12** (*16*). Scheme 2 shows the ODRC reaction of **12** to **19**, in which as many as 22 β-β bonds are formed in a one-pot reaction. The largest fused array, **19**, provides spacious coplanar π-electronic area with about 100 Å by 7 Å.

The electronic absorption spectra of the porphyrin **5**, the *meso-meso*–linked porphyrin arrays (**6** to **12**), and triply linked porphyrin arrays (**13** to **19**) taken in $CHCl_3$ are shown in Fig. 1. The absorption spectra of the *meso-meso*–linked porphyrin arrays show split Soret bands (B-bands), which can be qualitatively accounted for in terms of the exciton coupling that is originating from the Coulombic interactions between the transition dipole moments (*14*). These results indicate that electronic π-conjugation is disrupted in the array, probably as a result of the almost perpendicular conformation of the neighboring porphyrins.

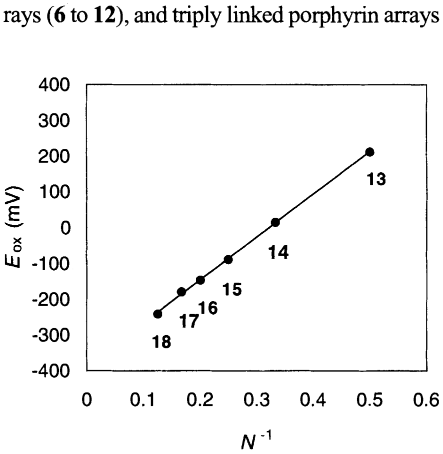

Fig. 4. Plot of the first oxidation potentials [E_{ox} (mV) versus $AgClO_4/Ag$ taken in $CHCl_3$] versus N^{-1}. The first oxidation potentials (E_{ox}) were obtained from cyclic voltammetry as follows: **13**, 212; **14**, 14; **15**, −89; **16**, −147; **17**, −180; and **18**, −241 mV. The oxidation potential of **19** could not be determined owing to its poor solubility. The line shown is represented by the equation $E_{ox} = 1197N^{-1} - 386$ (mV) with correlation coefficient $r^2 = 0.999$.

In sharp contrast, the triply linked fused porphyrin arrays display drastically red-shifted absorption spectra that reflect extensive π-conjugation over the array. The absorption spectra of the triply linked porphyrin arrays exhibit three distinct bands in $CHCl_3$ solutions as in the *meso-meso*–linked porphyrin arrays but at entirely different positions (designated as bands I, II, and III in Fig. 1). Although bands I are observed at 23,800 to 24,600 cm^{-1}—nearly the same positions as that of the monomeric $Zn^{(II)}$-porphyrin **5**—bands II and III are markedly red-shifted upon the increase in the number of porphyrins (*17*). A degree of saturation behavior is noted for the red-shift of bands II, whereas bands III exhibit a progressive red-shift of their peak positions upon the increase in the number of porphyrins as follows: **13** (dimer), 9400; **14** (trimer), 7500; **15** (tetramer), 6600; **16** (pentamer), 6000; **17** (hexamer), 5400; **18** (octamer), 4500; and **19** (dodecamer), 3500 cm^{-1}. Thus, bands III of **17**, **18**, and **19** are located in the IR region with their tails extending beyond 3000 cm^{-1}. A plot of the absorption peak of band III in wavelength units (λ_{max}) versus the number of porphyrins (N) revealed fairly linear behavior up to **19** without an indication of the ECL effect (Fig. 2). These results suggest a further possible decrease in the excitation energy of band III upon elongation of the array.

Strong electronic transitions enter the IR frequency region with their tails reaching ~1500 cm^{-1} for **17**, **18**, and **19** in solid states (Fig. 3). The relative amplitudes of the vibrational IR bands appear to decrease compared with the amplitude of the electronic absorption band (especially for the C-H stretching bands around 2900 cm^{-1}), probably because of the increasing relative intensity of the electronic transition upon the increase in the number of porphyrins. Detailed examination of the low-energy electronic absorption should provide important information on the vibronic coupling of organic molecules.

The first one-electron oxidation potential of the fused diporphyrin **4** is 0.11 V versus $AgClO_4/Ag$ in $CHCl_3$ solution (*13*), which is considerably lower than the values for the parent porphyrin monomer **5** (0.52 V) and *meso-meso*–linked diporphyrin **3** (0.47 V). Thus, the expansion of π-electronic system tends to raise the highest occupied molecular orbital (HOMO) orbital. This trend is increasingly enhanced upon the increase in the number of porphyrins as shown in Fig. 4, where a

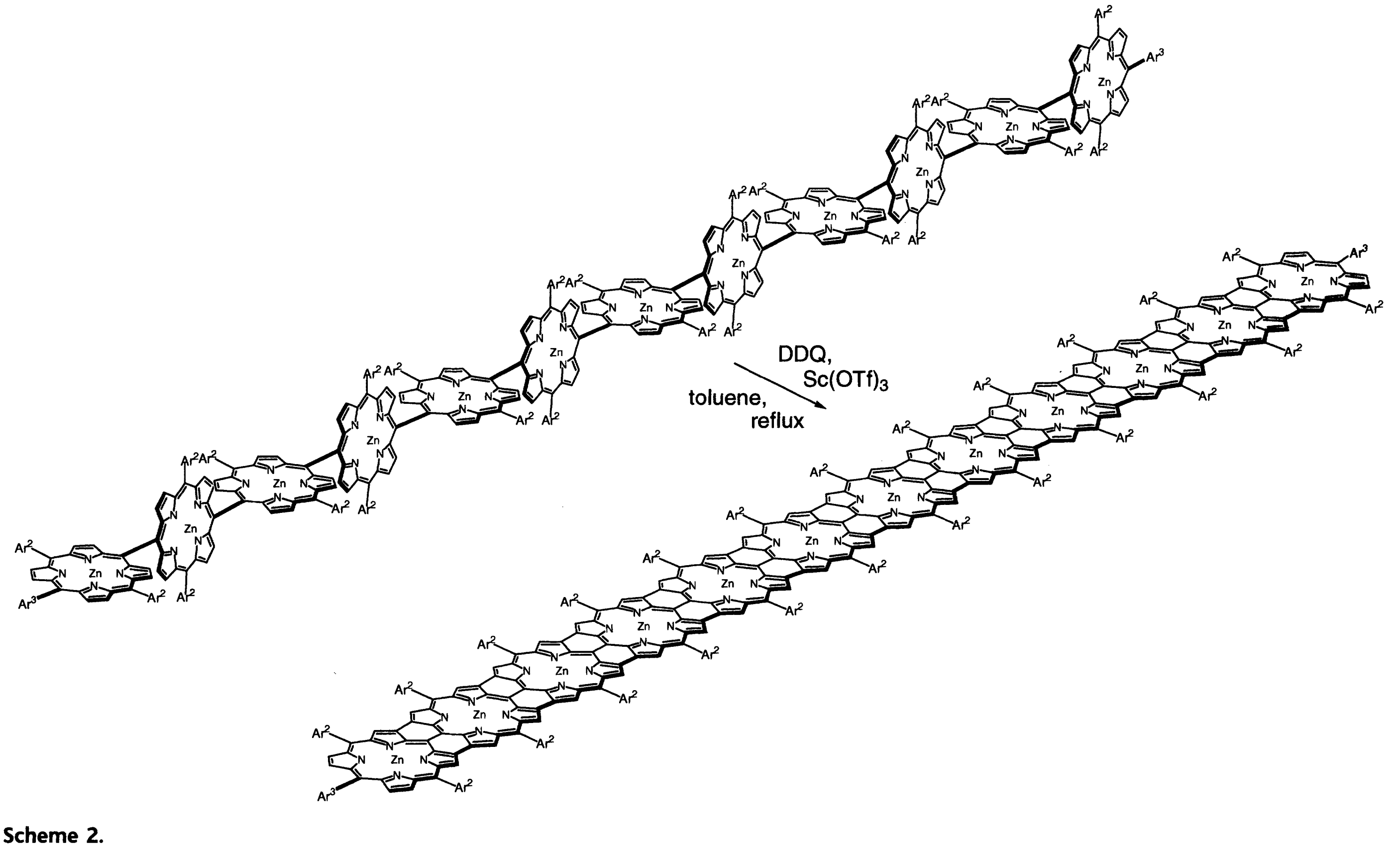

Scheme 2.

plot of the one-electron oxidation potentials versus N^{-1} exhibits good linearity. The intercept (−0.38 V) of the plot may be assigned for the one-electron oxidation potential of the "infinite" fused porphyrin polymer.

In spite of their remarkable properties, including extremely low HOMO-LUMO (highest occupied/lowest unoccupied molecular orbital) gaps, low one-electron oxidation potentials, and rigid and giant molecular size, the triply linked arrays are stable in air and easily manipulated, and should prove useful for studies on the vibronic coupling of organic molecules. They may also find use as conducting molecular wires and in molecular-scale electronic devices. In addition, the unusual photophysical and electrochemical properties of these fused porphyrin arrays suggest potential avenues for further investigation, including the development of near-IR and IR sensors and dyes, and materials for nonlinear optics and spin ordering.

References and Notes

1. R. E. Martin, F. Diederich, *Angew. Chem. Int. Ed.* **38**, 1351 (1999).
2. J. Chen, M. A. Reed, A. M. Rawlett, J. M. Tour, *Science* **286**, 1550 (1999).
3. G. Stegeman, P. Likamwa, *Nonlinear Optical Materials and Devices for Applications in Information Technology*, A. Miller, K. R. Welford, B. Daino, Eds. (Kluwer, Dordrecht, Netherlands, 1995), vol. 289, pp. 285–320.
4. E. Clar, *Ber. Dtsch. Chem. Ges.* **69**, 607 (1936).
5. H. Kuhn, *J. Chem. Phys.* **17**, 1198 (1949).
6. L. M. Tolbert, X. Zhao, *J. Am. Chem. Soc.* **119**, 3253 (1997).
7. D. P. Arnold, G. A. Hearth, *J. Am. Chem. Soc.* **115**, 12197 (1993).
8. V. S.-Y. Lin, S. G. DiMagno, M. J. Therien, *Science* **264**, 1105 (1994).
9. H. L. Anderson, *Chem. Commun.* 2323 (1999).
10. M. J. Crossley, P. L. Burn, *J. Chem. Soc. Chem. Commun.* 1569 (1991).
11. M. G. H. Vicente, L. Jaquinod, K. M. Smith, *Chem. Commun.* 1771 (1999).
12. A. Tsuda, A. Nakano, H. Furuta, H. Yamochi, A. Osuka, *Angew. Chem. Int. Ed.* **39**, 558 (2000).
13. A. Tsuda, H. Furuta, A. Osuka, *Angew. Chem. Int. Ed.* **39**, 2549 (2000).
14. N. Aratani, A. Osuka, Y. H. Kim, D. H. Jeong, D. Kim, *Angew. Chem. Int. Ed.* **39**, 1458 (2000).
15. Recently, we obtained the x-ray crystal structures for *meso-meso*–linked diporphyrin and triporphyrin, both of which display the almost perpendicular conformation of the neighboring porphyrins.
16. The shorter arrays **13**, **14**, and **15** were fully characterized by their ^{1}H nuclear magnetic resonance (NMR) and matrix-assisted laser-desorption/ionization time-of-flight (MALDI-TOF) mass spectroscopy (MS). It proved difficult to obtain satisfactorily resolved ^{1}H NMR spectra for longer arrays owing to their poor solubility, but their MALDI-TOF MS spectra indicated clustering peaks corresponding to dimers of ionized arrays. In the gel-permeation chromatography, all the triply linked porphyrin arrays exhibit a single band with a retention time that is progressively slower than those of the starting *meso-meso*–linked porphyrin arrays, indicating their discreteness and homogeneity. In addition, preliminary scanning tunneling microscopy measurements on these arrays revealed a roughly rectangular shape for hexamer **17** (2 nm by 5 nm) and octamer **18** (2 nm by 6.5 nm), consistent with the expected molecular shapes (*18*).
17. Although the assignment of these absorption bands (I, II, and III) has not yet been fixed, it may be possible to qualitatively understand these spectral characteristics on the basis of the well-established Gouterman four-orbital theoretical model for the absorption spectra of porphyrins (*19*, *20*). In this theory, the B and Q bands both arise from π-π^* transitions and can be explained in terms of a linear combination of transitions from a_{1u} and a_{2u} HOMO orbitals to a degenerate pair of e_{gx} and e_{gy} LUMO orbitals. The two HOMO orbitals have the same energy, and the configurational interaction results in two bands with very different intensities and wavelengths: the intense, short-wavelength B band and the weak, long-wavelength Q band. However, the fused connection causes a significant perturbation that breaks down the degeneracy of the e_{gx} and e_{gy} orbitals. It may thus be pertinent to assign the bands I and II to allowed transitions along the shorter and longer molecular axes of the rectangular fused porphyrin arrays, respectively. Band III may thus correspond to a formally forbidden transition such as Q-bands in the D_4-symmetry Zn(II) porphyrin monomer, because these absorption bands become increasingly intensified upon the increase of the arrays.
18. A. Takagi, Y. Yanagawa, T. Matsumoto, T. Kawai, A. Tsuda, A. Osuka, unpublished results.
19. M. Gouterman, *J. Mol. Spectrosc.* **6**, 138 (1961).
20. O. Bilsel *et al.*, *J. Am. Chem. Soc.* **114**, 6528 (1992).
21. Supported by Grants-in-Aid for Scientific Research from the Ministry of Education, Science, Sports and Culture of Japan (11223205, 12440196, and 12874076) and by CREST (Core Research for Evolutional Science and Technology) of Japan Science and Technology Corporation. A.T. was supported by a Japan Society for the Promotion of Science Research Fellowship for Young Scientists.

5 February 2001; accepted 22 May 2001

Approach to High-Resolution ex Situ NMR Spectroscopy

Carlos A. Meriles, Dimitris Sakellariou, Henrike Heise,
Adam J. Moulé, Alexander Pines*

Nuclear magnetic resonance (NMR) experiments are typically performed with samples immersed in a magnet shimmed to high homogeneity. However, there are many circumstances in which it is impractical or undesirable to insert objects or subjects into the bore of a high-field magnet. Here we present a methodology based on an adaptation of nutation echoes that provides resolved spectra in the presence of matched inhomogeneous static and radiofrequency fields, thereby opening the way to high-resolution ex situ NMR. The observation of chemical shifts is regained through the use of multiple-pulse sequences of correlated, composite *z*-rotation pulses, producing resolved NMR spectra of liquid samples.

The practice of high-resolution NMR spectroscopy usually involves the use of large magnets producing homogeneous static (B_0) fields. Experiments performed inside such magnets yield information about molecular structure and dynamics through the observation of interactions such as chemical shifts and scalar couplings. These features make in situ NMR a powerful analytical tool used to study such diverse questions as the metabolism of plants and organisms (*1*), the dynamics of geological processes (*2*), and the characterization of technologically important new materials (*3*). For many applications, it would be useful if a mobile magnet could be scanned over an otherwise inaccessible object or subject in order to acquire magnetic resonance information. The advantage of such ex situ analysis is that limitations of sample size

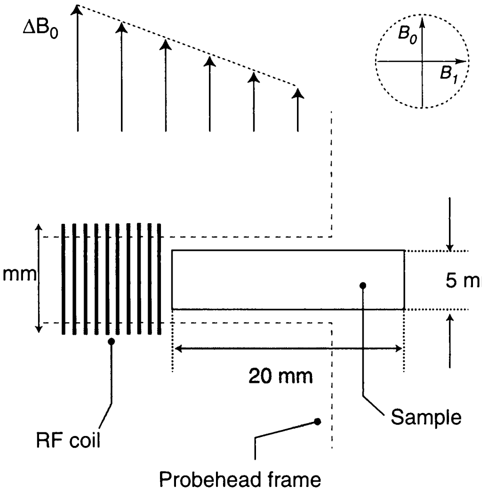

Fig 1. Schematic representation of the experimental setup. A single solenoid serves to irradiate and detect the NMR proton signal from a sample of trans-2-pentenal contained in a glass tube inside the bore of a superconducting magnet. To simulate the environment of an ex situ surface coil, we placed the sample completely outside the solenoid central cavity. An imaging coil set (not displayed in the figure) is used to generate a linear gradient of the static field along the solenoid axis. All experiments were carried out in a super-widebore imaging magnet with an Infinity Varian spectrometer operating at 179.12-MHz proton frequency and a home-built imaging probehead with three perpendicular gradient coils.

Materials Sciences Division, Lawrence Berkeley National Laboratory and Department of Chemistry, University of California, Berkeley, CA 94720, USA.

*To whom correspondence should be addressed.